© 2015. Published by The Company of Biologists Ltd | Journal of Experimental Biology (2015) 218, 3551-3558 doi:10.1242/jeb.123893

RESEARCH ARTICLE

Remora fish suction pad attachment is enhanced by spinule friction

Michael Beckert[1,‡], Brooke E. Flammang[2] and Jason H. Nadler[3,*,‡]

ABSTRACT

The remora fishes are capable of adhering to a wide variety of natural and artificial marine substrates using a dorsal suction pad. The pad is made of serial parallel pectinated lamellae, which are homologous to the dorsal fin elements of other fishes. Small tooth-like projections of mineralized tissue from the dorsal pad lamella, known as spinules, are thought to increase the remora's resistance to slippage and thereby enhance friction to maintain attachment to a moving host. In this work, the geometry of the spinules and host topology as determined by micro-computed tomography and confocal microscope data, respectively, are combined in a friction model to estimate the spinule contribution to shear resistance. Model results are validated with natural and artificially created spinules and compared with previous remora pull-off experiments. It was found that spinule geometry plays an essential role in friction enhancement, especially at short spatial wavelengths in the host surface, and that spinule tip geometry is not correlated with lamellar position. Furthermore, comparisons with pull-off experiments suggest that spinules are primarily responsible for friction enhancement on rough host topologies such as shark skin.

KEY WORDS: *Echeneis naucrates*, Asperity, Ratcheting friction, Adhesion

INTRODUCTION

Among known suction-based attachment mechanisms in fishes (Gibson, 1969; Green and Barber, 1988; Maie et al., 2012; Wainwright et al., 2013), the remoras (family Echeneidae) are the only group to have derived their suction apparatus from dorsal fin elements. The suction pad of remoras is homologous to the dorsal fin common to other bony fish species (Britz and Johnson, 2012). It has been suggested that attaching to mobile hosts benefits the remoras by reducing metabolic demands for swimming (Muir and Buckley, 1967), offering opportunistic feeding (Strasburg, 1962) or increasing the chance of finding mates (Silva and Sazima, 2003). Remoras have been known to strongly attach to sharks (Ritter, 2002; Ritter and Brunnschweiler, 2003), rays (Williams et al., 2003), other pelagic fish (Williams et al., 2003), sea turtles (Sazima and Grossman, 2006), dolphins (Weihs et al., 2007), divers (Silva and Sazima, 2003), buoys (Cressey and Lachner, 1970), ship hulls (Cressey and Lachner, 1970) and concrete (Strasburg, 1962). This variety of hosts moves at many different speeds and have body surfaces that span a broad spectrum of geometries and topologies (Stote et al., 2014). Despite this remarkable behavior, there has not been experimental confirmation of the underlying mechanisms or any numerical analyses of the physical forces that contribute to this attachment function.

A remora (*Echeneis naucrates* Linnaeus 1758) pad has several distinct features that work in concert to achieve reversible attachment: the outer fleshy lip, an array of lamellar compartments (Fig. 1A) and spinules that protrude from the individual lamella (Fig. 1B). A remora has thousands of these spinules on its dorsal pad, spaced several hundred micrometers apart (Nadler et al., 2013). They project from the lamella and terminate as cone-like, blunted points as shown by the scanning electron microscope (SEM) image in Fig. 1C (Nadler et al., 2013). Whereas the fleshy lip and lamellar compartments are thought to play significant roles in creating a suction seal and bonding (Barnes, 2007) to the host (Culler et al., 2014; Culler and Nadler, 2014), spinules are believed to provide a friction enhancement function (Hora, 1923; Sewell, 1925; Fulcher and Motta, 2006). In previous experiments, where attached remoras were dislodged from both smooth Plexiglas and shark skin (Fulcher and Motta, 2006), removal from shark skin required significantly greater posterior-directed loads, despite the higher suction pressures measured on Plexiglas. By pressing their spinules against the host (contact surface), the remora is thus able to resist slippage during hitchhiking. An increased friction coefficient between the remora and its host would allow the remora to withstand larger drag forces induced by host locomotion without slipping. Furthermore, because friction is passive, it would be an efficient means to increase shear resistance without requiring increased effort on the part of the remora.

Unfortunately, directly measuring friction across multiple length scales is extremely challenging in a biological system, making modeling of the interfacial action necessary to understand the mechanics behind shear resistance by the remora. On a global (macroscopic) scale, friction is manifested as the resistance of motion between two contacting surfaces (Bowden and Tabor, 1950), in this case between the disc of the remora and the skin of the host. It is often characterized by a dimensionless friction coefficient defined as the ratio of the friction and normal forces. At the interface between mating materials, local asperities (peaks resulting from surface roughness), such as those on the skin of the host, can play an essential role in friction. For example, in systems where a stylus slides along a hard surface or when one surface is in contact with much rougher surface of approximately equal hardness, a 'ratchet' mechanism exists whereby local asperities move past and climb over one another either during (dynamic friction) or at the initiation (static friction) of sliding (Makinson, 1948; Bowden and Tabor, 1950; Bhushan and Ruan, 1994; Bhushan, 2002). In theory, with respect to the remora, when spinules (the styli) make contact with a rough host surface (asperities), the local asperities interlock with the spinules, resulting in increased friction.

[1]Woodruff School of Mechanical Engineering, Georgia Institute of Technology, Atlanta, GA 30332, USA. [2]Department of Biological Sciences, New Jersey Institute of Technology, Newark, NJ 07102, USA. [3]Electro-Optical Systems Laboratory, Georgia Tech Research Institute, Atlanta, GA 30332, USA.
[‡]Present address: Advanced Concepts Laboratory, Georgia Tech Research Institute, Atlanta, GA 30332, USA.

*Author for correspondence (jason.nadler@gtri.gatech.edu)

Received 17 April 2015; Accepted 4 September 2015

Journal of Experimental Biology (2015) 218, 3551-3558 doi:10.1242/jeb.123893

List of symbols

a,b,c,d	constants for spinule termination best-fit plane
A	peak amplitude
$C(\omega)$	power spectral density
D	matrix for determining best-fit plane constants
$\vec{F}_F$	friction force between local asperity and spinule
$\vec{F}_N$	normal force between local asperity and spinule
$\vec{F}_P$	shearing force on spinule aligned with global horizontal axis
$\vec{F}_W$	contact force on spinule aligned with global vertical axis
h	surface height
$\bar{h}$	mean surface height
L	spatial wavelength or peak spacing
L_0	cut-off wavelength
R	spinule tip radius
R_q	root mean square surface roughness
u,v	surface-mapping parameters
x, y, z	spatial coordinates
α,β	fitting constants for power spectrum
θ	local asperity slope
μ_0	local friction coefficient
μ	global friction coefficient
ω	spatial frequency

At the local (microscopic) scale, asperities increase the shearing force, $\vec{F}_P$, on a spinule required to overcome the friction force $\vec{F}_F$ by increasing the slope of the contact surface θ with respect to the applied contact force $\vec{F}_W$, seen in Fig. 2A. Balancing the forces in Fig. 2A and employing the usual definition of friction, Eqn 1 (Bowden and Tabor, 1950; Bhushan, 2002) relates the local (μ_0) and global (μ) friction coefficients. The local friction coefficient represents the true adhesive friction coefficient occurring between a spinule and an asperity, whereas the global friction coefficient represents the observed coefficient aligned with the global vertical and horizontal axis (Bhushan, 2002). With respect to the remora, shearing forces may be induced by drag associated with host locomotion, whereas contact forces may be supplied by suction and the elasticity of the remora's soft tissues. However, Eqn 1 states that regardless of the origins of the contact ($\vec{F}_W$) and shearing ($\vec{F}_P$) forces, only knowledge of the local friction coefficient (μ_0) and surface slope (θ) are required to estimate the global friction coefficient (μ). This treatment of friction assumes that at the length scale under investigation, the phenomenological causes of friction are taken into account by the local friction coefficient:

$$\mu = \frac{\vec{F}_P}{\vec{F}_W} = \frac{\mu_0 + \tan\theta}{1 - \mu_0 \tan\theta}, \text{ with } \mu_0 = \frac{\vec{F}_F}{\vec{F}_N}. \quad (1)$$

In practice, finding the appropriate slope needed for the ratcheting friction model can be a challenge. Real surfaces are complex and formed by a spectrum of asperities with varying heights and separation distances. Furthermore, real spinules are not capable of entering and traversing every skin surface valley because they are not infinitely sharp. This illustrates the need to consider both the topological spectrum of the contact or host surface and the shape of the spinule tip when determining the slope needed for the ratcheting friction model. Here, both of these features are taken into account by considering the power spectrum of the host surface and the actual 3D spinule tip shape.

In addition to the slope, the distance between asperity peaks or spatial wavelength L also plays an important role in friction, as the spinule tip must be able to enter the valleys between asperities to enhance friction. For example, when the slope (θ) is large and the gap between peaks (L) is small with respect to the spinule tip radius R, the contact surface appears flat with respect to the spinules. In this case, the spinules alias the surface as they only touch the asperity peaks. This causes the local and global coefficients of friction to converge (Fig. 2B). The converse is also important because a small slope (θ) and large gap (L) with respect to tip radius (R) renders the asperities effectively flat in which case the local and global coefficients of friction again converge (Fig. 2C). Although both of these scenarios suggest methods for obtaining the local friction coefficient, difficulty arises when working with natural tissues as altering structures to obtain flat tips (large R) or flat substrates (large L) exposes underlying tissues not normally present at the contact interface. For this reason, measuring local friction between the

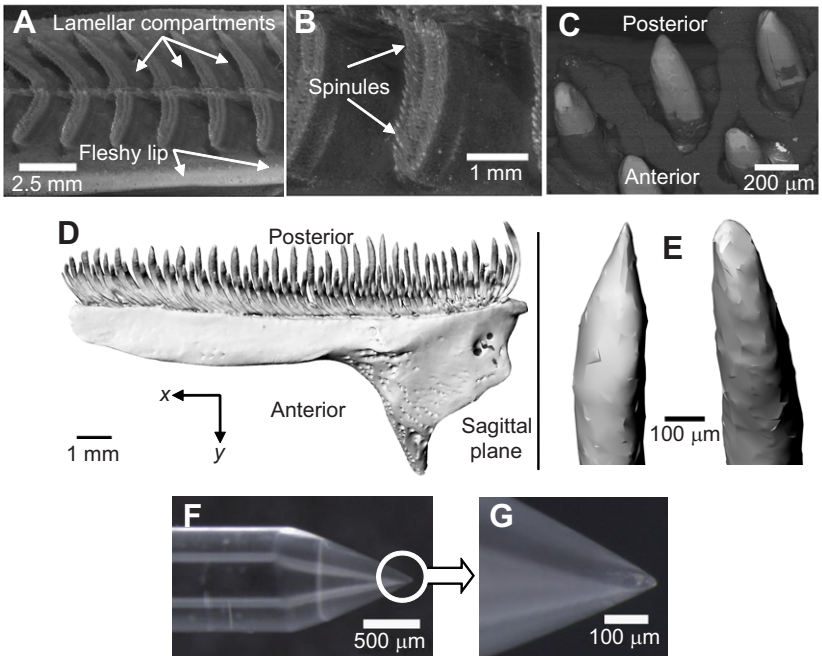

Fig. 1. Structures of the suction disc in the remora *Echeneis naucrates*. (A,B) Optical microscope images of the remora suction disc show the pad's functional features (anterior is to the right and posterior is to the left). (C) SEM image of spinules protruding from suction disc (Nadler et al., 2013). (D) A µCT scan of an individual lamella shows its many spinules that vary in tip shape (E). Optical microscope image of an artificial spinule fabricated from glass (F) and its tip shape (G).

Journal of Experimental Biology

Journal of Experimental Biology (2015) 218, 3551-3558 doi:10.1242/jeb.123893

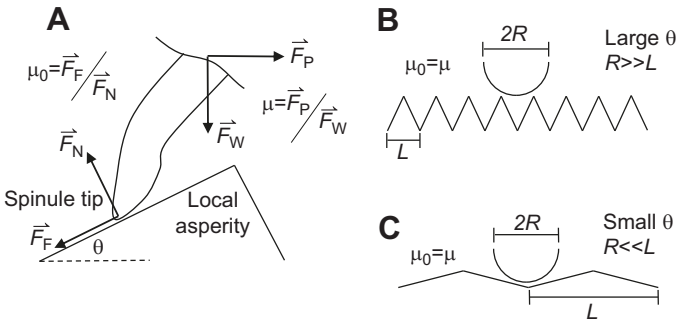

Fig. 2. Local asperities on a surface play a critical role in friction when a stylus slides over a surface of approximately equal hardness. (A) An idealized free body diagram of a spinule tip on a local asperity shows the true adhesive friction (local) coefficient (μ_0) is related to the observed (global) friction coefficient (μ) by the slope (θ) of local asperities relative to the spinule tip. (B) A spinule tip aliases the host surface when asperities are closely spaced. (C) Asperities occurring at long wavelengths, *L* (peak spacing), are effectively flat with respect to the spinule tip.

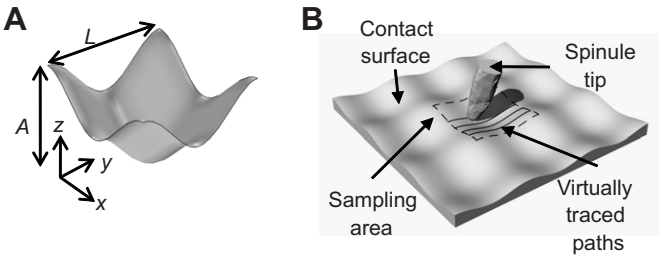

Fig. 3. Using a spinule to probe surface roughness, one wavelength at a time. (A) A single wavelength and amplitude component from the contact surface's spectrum is parameterized by the periodic, repeating surface (*L*, spatial wavelength or peak spacing; *A*, peak amplitude). A three-dimensional contact analysis is performed over all the components in the power spectrum, whereby (B) individual spinules trace (solid lines) a single period (broken lines) of a component to determine the local slope at the interface.

spinules and a host surface in a living system would be exceedingly difficult.

The current work aims to describe the effect of surface roughness on friction at the interface between an attached remora and its host. The contribution of the spinules to attachment is described by applying a friction model to the interaction of spinule tips and a host's surface topology. The spinules were treated as individual styli that ratchet over host surface asperities. A 3D model of friction was developed that considers the geometry of remora spinules obtained from micro-computed tomography (μCT), and host surface topology measurements from confocal microscopy. Model results were compared with directly measured friction coefficients of both natural and synthetic spinules on glass substrates with prescribed roughness. Finally, the macroscopic friction that developed between remora spinules and shark dermal denticles was used to investigate whether spinule geometry is affected by its position within the lamella.

MATERIALS AND METHODS

Characterization of rough contact or host surfaces

Contact surface topology was characterized by its radially averaged power spectrum, $C(\omega)$. The power spectrum decomposes a surface into its individual amplitude A and spatial frequency ω (or wavelength $L=2\pi/\omega$) components (Vorburger, 1992). The amplitude at a particular frequency can be related to the spectral intensity using:

$$A(\omega) = \sqrt{2}C(\omega)^{\frac{1}{4}}. \quad (2)$$

Often, the power spectrums of real surfaces obey a power law relationship with respect to spatial frequency (Persson et al., 2005), as seen where α and β are fitting constants:

$$C(\omega) = \alpha\omega^{\beta}. \quad (3)$$

When the amplitude and wavelength components were combined in Eqns 4–6, the contact surface at a particular spatial wavelength was represented by the periodic surface shown in Fig. 3A, where u and v are mapping parameters and x, y, and z are spatial coordinates:

$$x = uL, \quad (4)$$

$$y = vL, \quad (5)$$

$$z = A(\cos 2\pi u + \cos 2\pi v),\ u, v \in [0, 1]. \quad (6)$$

This representation of the rough surface was used to calculate its average slope with respect to the spinules for a range of individual wavelengths across its spectrum. This allowed for the identification of asperity heights and wavelengths that most contributed to friction enhancement.

The topology of the roughened surfaces was measured using an LEXT OLS4000 3D material confocal microscope (Olympus, Tokyo, Japan). The FFTs and power spectrums of the roughened substrates were computed from height maps in Matlab (R2009a, Natick, MA, USA) using methods outlined by Persson et al. (2005). As a check of numerical accuracy, the root mean square roughness R_q was computed directly from measured height data and the power spectrum fit. Eqn 7 relates R_q to the computed power spectrum in Eqn 3 and the measured height data h, where N is the number of data points, $\bar{h}$ is the average height and L_0 is the cut-off wavelength:

$$R_q^2 = 2\pi \int_{2\pi/L_0}^{\infty} C(\omega)\omega d\omega = \frac{1}{N}\sum_i (h_i - \bar{h})^2. \quad (7)$$

The frequency and amplitude components of shark skin needed to parameterize the contact surface were obtained from confocal microscope data of a shortfin mako (*Isurus oxyrinchus*) in Culler et al. (2014). Shortfin mako was chosen because it was a readily available fresh tissue specimen; preserved specimens generally had significant distortion from the preservation process.

Spinule tip geometry and the ratcheting friction model

As seen in Fig. 1C, spinules are geometrically complex, and thus are not well suited for a single parameter description; therefore, the full 3D geometry was taken into account here. Working in Rhinoceros 3D (v5, Seattle, WA, USA), individual spinules and tip locations were identified using algorithms developed in Nadler et al. (2013). An interesting feature observed with respect to the spinules was that for an individual lamella, all of the spinules terminated in approximately the same plane despite differences in respective spinule lengths. This plane provided a natural and objective orientation for the lamella and spinules. The equation of a plane is given by Eqn 8, where x, y, z are the respective spatial coordinates:

$$ax + by + cz = d. \quad (8)$$

The best-fit plane was found in a least squares sense by computing the eigenvectors of the matrix D, which was built from the respective spinule tip locations (x_i, y_i, z_i) as seen in Eqn 9. The plane's normal vector was formed directly from the constants a, b, and c of the appropriate eigenvector:

$$\begin{bmatrix} x_i & y_i & z_i & -1 \end{bmatrix}^{\mathrm{T}} \begin{bmatrix} x_i & y_i & z_i & -1 \end{bmatrix}$$
$$\begin{bmatrix} a & b & c & d \end{bmatrix}^{\mathrm{T}} = [D]\begin{bmatrix} a & b & c & d \end{bmatrix}^{\mathrm{T}} = 0. \quad (9)$$

Using the spinule tip locations, individual tip geometries were isolated as seen in Fig. 3B. Isolated spinule tips were used to virtually sample (or trace) a range of individual spatial wavelength components within the contact surface's spectrum, as described by Eqn 6. Because of the periodicity of Eqn 6, only one period of the contact surface was sampled (broken lines in

Journal of Experimental Biology (2015) 218, 3551-3558 doi:10.1242/jeb.123893

Fig. 3B). After sampling the contact surface at a particular wavelength, the slopes along the virtual traces were determined. The average global friction coefficient was estimated by plugging the slopes from sampled points and the local friction coefficient into Eqn 1, and then averaging over one period of the contact surface (Bhushan, 2002). The result of the calculation was the average global friction coefficient versus the spatial wavelength component of the contact surface.

Once the friction analysis was performed on each individual spinule, a correlation analysis was performed to evaluate whether spinule position on the lamella was associated with friction enhancement. A coordinate system was drawn with the *x*-axis perpendicular and the *y*-axis parallel to the sagittal plane (plane of bilateral symmetry), where both axes lied in the plane of best fit, as seen in Fig. 1D. The analysis compared the global coefficient of friction computed for each spinule to both its respective *x* and *y* coordinates on the lamella.

Friction measurement

Friction coefficients were measured for both natural and artificial spinules on rough and smooth glass substrates with known topology. Friction measurements from the smooth surface provided values of the local friction coefficient (μ_0) because the local and global friction coefficients (μ) are equivalent on smooth surfaces (θ=0 in Eqn 1). By measuring both friction coefficients and surface topology, ratcheting friction model predictions were directly validated.

The contact surfaces used for testing were created from borosilicate glass substrates. Borosilicate glass was chosen because of its high stiffness and negligible plasticity to ensure the spinules operate in the ratcheting friction regime. Glass was obtained as an optically flat substrate, which provided a smooth surface. Rough surfaces were created by grinding glass substrates with 60 grit abrasive paper (Allied High Tech Products, CA, USA) on a wet polishing wheel (TwinPrep 3, Allied High Tech Products). All surfaces were cleaned with acetone and deionized water in a sonicating bath prior to testing.

Artificial spinules (Fig. 1F,G), were created from borosilicate glass rods to ensure they were of similar hardness to the substrates. The rods were drawn down to diameters (approximately 650 µm) comparable to natural spinules. The tips were created by grinding the drawn rods to a point using successively finer grit abrasive paper (max 1400 grit) on a wet polishing wheel. Three artificial spinules were mounted to a block in a tripod formation to ensure each would maintain contact with the substrate.

Natural spinules were provided by a fixed remora (*Echeneis naucrates*) specimen (Nadler et al., 2013). Only the spinules of the specimen made contact with the test substrates as the fixing process rendered them erect and free from soft tissue interference as seen in Fig. 1. The tip geometries of 92 spinules were obtained from a high-resolution µCT scan of an individual lamella seen in Fig. 1D (Culler et al., 2014). For the interface between remora and shark skin, it was not possible to measure the local friction coefficient between denticles and spinules directly as altering the natural geometry would have exposed underlying tissues of the denticles with differing local properties than the outer surface. However, the global coefficient of friction for remora and shark skin was computed from measured data in Fulcher and Motta (2006), which yielded a value of approximately 0.22±0.07. The local friction coefficient was obtained by iteratively solving the friction model with different local friction coefficient inputs until the desired global friction coefficient was obtained.

Friction coefficients were measured using the apparatus shown in Fig. 4 conforming to ASTM D1894 (ASTM, 2014). Prior to testing, a film of storage solution from the remora specimen (1× phosphate buffer) was manually applied to the substrate to both simulate the remora's fluid environment and provide consistency between trials. A lightweight, flexible, low-stretch cord connected the test specimen to a force gauge (Mark-10M5-20, Copiague, NY, USA) through a low-friction pulley. The force gauge's displacement was controlled by a test frame (Mark-10 ESM301, Copiague), and in each test, the gauge moved at constant velocity (75 mm min^{-1}). Friction coefficients were computed as the force measured by the gauge divided by the combined force of the specimen's weight (37.7 g) and any added weights, as in Eqn 1. The remora's mass changed by less than 1% during testing, and all tests were carried out at 25°C.

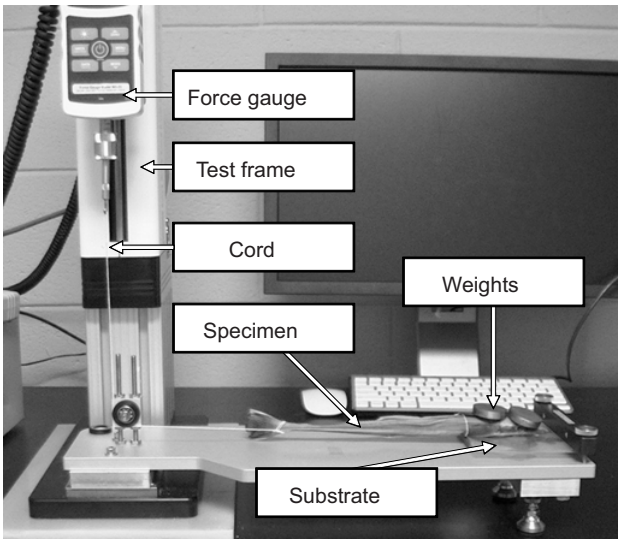

Fig. 4. Displacement-controlled force-measurement system used to determine friction coefficients. Apparatus is shown operating with a remora specimen.

RESULTS

Contact surfaces

Height data from confocal microscopy of the roughened glass substrate is seen in Fig. 5A. The corresponding FFT is shown in the inset and clearly displays circular symmetry. The power spectrum, of the roughened glass substrate investigated is seen in Fig. 5C. The exponential decay of the power spectrum is evident as the intensity of the roughness drops linearly (R^2=0.9913) with respect to spatial frequency on a log–log scale. Excellent agreement was observed between the directly computed root mean square surface roughness (2.99 µm) and integration of the power law approximation (2.95 µm) with Eqn 7 at the cut-off wavelength (369 µm).

The height data from the denticle surface of a shortfin mako shark is shown in Fig. 5B with the corresponding 2D FFT inset. The surface's radially averaged power spectrum along with its posterior directed component is shown in Fig. 5C (Culler et al., 2014). Although the FFT shows a slight departure from isotropy along its horizontal axis (due to the denticle ridges), there remains a large amount of overlap between the radially averaged and posterior-directed power spectra. This indicates that the averaged spectrum is a reasonable approximation of the shark skin in Fig. 5B for the purposes of analyzing posterior-directed friction. Similar to the roughened glass substrate, the averaged power spectrum decays exponentially with increasing frequency, as evidenced by the linear (R^2=0.9948) trend on a log–log scale. Excellent agreement was observed between the directly computed root mean square surface roughness (10.50 µm) and integration of the power law approximation (10.48 µm) with Eqn 7 at the cut-off wavelength (236 µm).

Friction measurements and ratcheting model

Spinule tip shape was needed to apply the ratcheting friction model. Optical micrographs in Fig. 1F,G show the tip geometry of the artificial spinules. Fig. 1D shows the tip geometry of 92 natural spinules provided by µCT scanning when viewed from above the best-fit plane with the *x*-axis perpendicular and the *y*-axis parallel to the sagittal plane. These tip geometries were used in the ratcheting friction model to determine the minimum wavelength they were capable of entering before peak aliasing occurred, as in Fig. 2B.

Journal of Experimental Biology

Journal of Experimental Biology (2015) 218, 3551-3558 doi:10.1242/jeb.123893

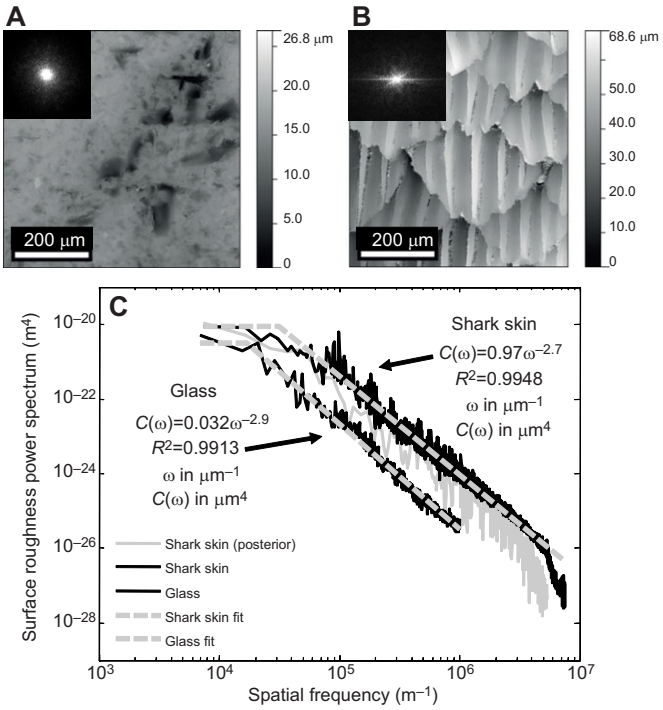

Fig. 5. Confocal microscopy height map and power spectrum data. Height maps are shown for (A) the roughened glass substrate and (B) the denticle surface of a shortfin mako shark (*Isurus oxyrinchus*) with their corresponding two-dimensional FFTs (insets). (C) Power spectra corresponding to the height maps.

The friction coefficients of both natural and artificial spinules on the smooth and roughened glass substrates were directly measured. Using the substrate topology, spinule tip geometries, and local friction coefficients (μ_0) measured on smooth surfaces, the global friction coefficients (μ) predicted by the ratcheting friction model were compared with corresponding friction measurements on rough surfaces. A summary of the friction coefficients determined by the ratcheting model and those directly measured is shown in Table 1.

Measurements using the artificial spinules on the smooth and roughened glass substrates are shown in Fig. 6A with respect to the displacement of the force gauge. After the initial rise in the friction coefficient preceding slip, the artificial spinules exhibited uniform sliding as evidenced by the nearly constant friction coefficient (0.122±0.006) on the smooth surface. In contrast, on the rough surface, the artificial spinules moved in a 'stick-slip' fashion as evidenced by rapid fluctuations in the friction coefficient (0.35±0.04). With a local coefficient of 0.122, the tip geometry from Fig. 1G, and the power spectrum from Fig. 5C, the ratio of the global to local friction coefficient (μ/μ_0) as predicted by the ratcheting friction model for the artificial spinules on the rough substrate is shown in Fig. 6C. A comparison between the actual tip geometry from Fig. 1G to a theoretical tip of infinite sharpness is also shown in Fig. 6C. At shorter wavelengths (less than 34 μm), the frictional responses of the theoretical and actual tips diverge markedly, as the theoretical tip asymptotically approaches infinity whereas the actual tip geometry approaches one. This indicates the onset of peak aliasing. Conversely, at longer wavelengths, it can be seen that the theoretical and actual tips predicted equivalent friction enhancement (μ/μ_0). The peak value of friction enhancement in Fig. 6C (2.6±0.1) compared favorably with the measured increase in friction from the smooth to roughened substrate in Fig. 6A (2.9±0.4).

Friction coefficients from actual remora spinules behaved similar to artificial spinules on the glass substrates (Fig. 6B). After the initial rise preceding slip, the dead remora slid uniformly along the smooth substrate with a nearly constant coefficient of friction (0.081±0.002). On the rough surface, visual detection of the specimen's stick-slip motion was more difficult compared with the artificial spinules; however, fluctuations in the friction coefficient (0.24±0.01) are clearly visible. With a local friction coefficient of 0.081, the spinule tip geometries from the μCT data in Fig. 1D, and the power spectrum from Fig. 5C, the ratio of μ/μ_0 as predicted by the ratcheting friction model for remora spinules on the roughened substrate is shown in Fig. 6D. Again, at longer wavelengths, the theoretical infinitely sharp and actual tip geometries predicted equivalent friction enhancement, but diverged sharply at shorter wavelengths. The peak value of friction enhancement in Fig. 6D (3.3±0.5) occurred at approximately 38 μm, and compared favorably to the measured increase from Fig. 6B (3.0±0.2).

Fig. 6F shows the ratio μ/μ_0 as predicted by the ratcheting friction model using the spinule geometry from Fig. 1D, the denticle power spectrum data from Fig. 5C, and a local friction coefficient of 0.017. In contrast to both the previous cases where spinule friction was analyzed on glass substrates, the local friction coefficient was not known beforehand, but was calculated from the global friction coefficient (0.22±0.07) obtained from pull-off tests performed in Fulcher and Motta (2006). The similarities and differences between the actual spinule tips and infinitely sharp tips follow the same trends as observed in previous cases. Namely, they are equivalent at longer wavelengths, and diverge at shorter wavelengths. The peak of friction enhancement (13±3) occurred at approximately 100 μm.

From the correlation analysis, no significant association was found between the global friction coefficient (on shark skin) of each individual spinule within the lamella to their positions with respect to the x (r=0.103, N=92, P=0.326) and y (r=0.033, N=92, P=0.754) axes shown in Fig. 1D.

DISCUSSION

Although remoras are typically recognized for their strong suction seal, suction is not resistant to shear, and remoras attached to fast-moving hosts experience exceptionally high drag and shear loads. To guard against failure, the high number of engaged spinules increases friction on rough surfaces. The most important geometric property of spinules (with respect to friction) was shown to be tip shape because it determines the minimum wavelength that a spinule can access on a surface. This was borne out by the ratcheting friction model results seen in Fig. 6, as in each case maximum friction enhancement occurred at the minimum wavelength accessible by the spinule tips which corresponded to the measured friction enhancement. This is consistent with observations made by

Table 1. Summary of friction measurements and simulations

Spinule type	Smooth substrate, μ_0	Rough substrate, μ	Ratio (μ/μ_0)	Predicted ratio (μ/μ_0)
Artificial (glass/glass)	0.122±0.006	0.35±0.04	2.9±0.4	2.6±0.1
Natural (tissue/glass)	0.081±0.002	0.24±0.01	3.0±0.2	3.3±0.5
Natural (from Fulcher and Motta, 2006)	0.07±0.01 (tissue/Plexiglas)	0.22±0.07 (tissue/shark skin)	–	–

Journal of Experimental Biology (2015) 218, 3551-3558 doi:10.1242/jeb.123893

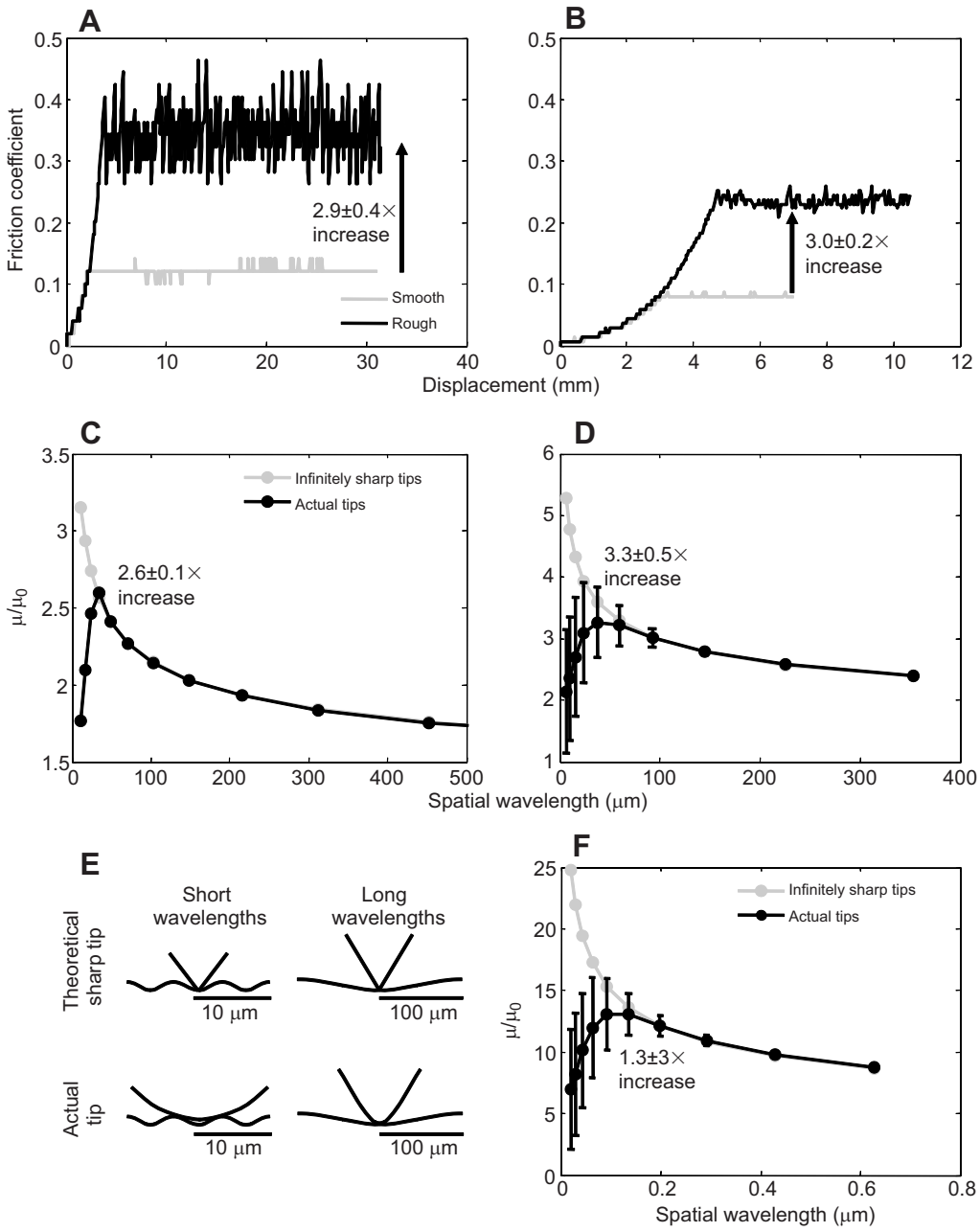

Fig. 6. Ratcheting friction model results and measured friction coefficients. Measured friction coefficients of (A) artificial and (B) natural spinules on rough and smooth glass substrates. Ratio of global to local friction coefficients (μ/μ_0) predicted by the ratcheting friction model using (C) the artificial and (D) the natural spinule geometries on the roughed glass topology. (E) An infinitely sharp tip compared with the actual tip geometry of the artificial spinules at short and long wavelengths. (F) Ratio of global to local friction coefficients predicted for natural spinules on shark denticle surface.

Bhushan and Ruan (1994) based on the fact that shorter wavelengths tend to dominate the slope of surface features for surfaces having a power spectrum of the form given by Eqn 3 (Persson et al., 2005). This effect is best visualized in Fig. 6E by comparing the friction developed by the infinitely sharp tip to the actual tip at long and short wavelengths. At long wavelengths – for example, a host with relatively smooth skin – there is little visible difference between the two tips and both are equally capable of entering surface valleys. However, the slope of surface features is small, resulting in minimal friction enhancement (Eqn 1). Conversely, at shorter wavelengths – for example, densely packed, very rough scales – the actual tip geometry appears almost flat compared with the contact surface, whereas the infinitely sharp tip is still able to fit between surface peaks and take advantage of the increased slope therein. Hence, at shorter wavelengths, sharper tip geometries can develop larger global friction coefficients.

Considering the importance of tip shape, distinct variations in sharpness were observed among the remora spinules investigated (Fig. 1E). The ratio of global to local friction coefficients (μ/μ_0) from the ratcheting friction model with respect to the 92 spinules, Fig. 6D,F depict increased uncertainty at shorter wavelengths. Because shorter wavelengths dominate the contribution to friction, it is reasonable to attribute the increased spread in the friction model data to variance in spinule geometry. Conversely, at longer wavelengths, the spread in the data was reduced, or in other words, spinule geometry was of less importance on smoother surfaces. This is also supported by the lack of fluctuation in the measured friction coefficients on smooth surfaces versus rough surfaces as seen in Fig. 6A and B, as no interlocking between spinules and the contact surface can occur on smooth surfaces.

Despite the importance of tip shape, the correlation analysis revealed no connection between friction enhancement and lamellar

Journal of Experimental Biology (2015) 218, 3551-3558 doi:10.1242/jeb.123893

position among the spinules investigated. Based on previous discussion, it follows that there is likely little correlation between spinule tip geometry and lamellar location. Thus, although spinule tip geometry does play a key role in friction enhancement, the sharpness or bluntness of a spinule does not appear to be related to its position within the lamella. As a result, any position of the lamellae carries spinules of a variety of tip ends, making it likely that at least some of the spinules in that region will be of the correct shape to interact with the asperities of a given host. Therefore, the observed variability in spinule geometry would result in a broad range of host roughness against which the remora can generate friction.

In terms of the optimal surface for remora attachment, the ratcheting friction model suggests that rougher surfaces are preferable as they provide increased shear and drag resistance. However, the suction-based attachment strategy employed by remoras requires the formation of a leak-proof seal, which is facilitated by smoother attachment surfaces (Culler et al., 2014). Therefore, any attempt to determine the optimal surface for remora attachment requires a fitness function that balances these competing goals with remora ecology; a topic worthy of future exploration.

An important similarity between the pull-off experiments in Fulcher and Motta (2006) and those made here on the dead remora was the stick-slip motion of spinules as evidenced by the rapid fluctuations of the friction coefficient with displacement (Fig. 6B). This provides evidence to support that ratcheting friction is occurring (spinules interlocking and sliding over local asperities) in both live and dead remora. Additionally, although the local friction coefficient computed for shark skin (0.02) here cannot be directly compared with measurements made on smooth Plexiglas (0.07±0.01 in Fulcher and Motta, 2006) because of material differences, the values are within the same order of magnitude. Nevertheless, all the measurements show a marked decrease in friction with surface roughness, and when the local friction coefficient could be determined, the ratcheting friction model presented here did predict the increased friction with reasonable accuracy (Fig. 6).

The most prominent feature of the friction analysis for the remora on shark skin in Fig. 6F was that the shark skin's roughness and the spinule geometries resulted in approximately an order of magnitude increase (13 times) in the global friction coefficient. This is an important adaptation for the remora because during hitchhiking, the remora must be able to resist drag forces induced by host locomotion, and increasing the contact force or suction pressure is the only mechanism available to the remora to do so. Increasing the friction coefficient by an order of magnitude permits the same friction force, and therefore drag resistance, to be obtained with an order of magnitude less suction pressure. This represents a significant energy saving to the remora, particularly if suction pressure is controlled by muscular activity or if the act of re-establishing suction jeopardizes attachment.

In addition to energy savings, the increase in friction force should also allow the remora to remain attached to its host at increased host swimming speeds and during maneuvers. In fact, several studies have observed blacktip shark (*Carcharhinus limbatus*) swimming behavior with remoras attached and found that remoras are typically dislodged by impact with either the ocean surface following re-entry after a host jump, with the ocean bottom, or on rocks rather than by swimming accelerations (Ritter, 2002; Ritter and Brunnschweiler, 2003). This is an impressive feat of friction for the remora considering blacktip sharks can reach swimming speeds as high as

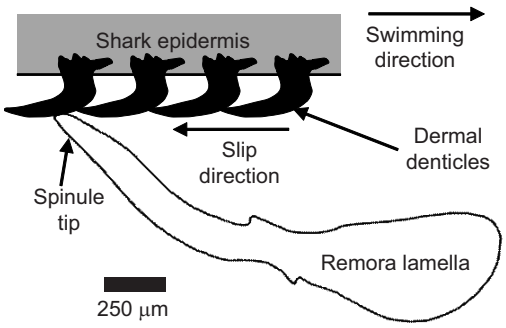

Fig. 7. Illustration of a spinule contacting overlapping dermal denticles. Anterior is to the right and posterior is to the left.

3.9 (Webb and Keyes, 1982) to 6.3 (Brunnschweiler, 2005) m s^{-1} at which speeds an attached remora would be moving at 8–12 body lengths per second.

A caveat of the analysis presented is that although dermal denticles themselves are quite stiff, the underlying epidermis (Fig. 7) is compliant, which allows some motion of the denticles (Motta et al., 2012). Although the spinules were treated individually with respect to friction, they are affixed to the lamellae, which are appreciably larger (1–10 mm) than individual denticles (100–300 μm). Thus, it seems somewhat unlikely that individual spinules could burrow deeply between denticles. However, if the denticles were forced erect under the influence of the remora's suction, similar to how remora are known to disturb their attachment site on a scaly hosts (Schwartz, 1977, 1992), this could have the effect of further increasing the roughness of the surface, which could result in increased friction coefficients based on the analysis presented. This may help to explain some of the attachment site fidelity observed in remoras (Strasburg, 1962).

Finally, although this work is focused solely on the friction created by spinules on relatively hard/rough surfaces, it remains that soft tissue from the remora pad also makes contact with the host surface in nature. When a material with viscoelastic properties like remora soft tissue (Culler et al., 2014) makes contact with a rough surface, the resulting friction is often a function of the energy dissipation mechanisms associated with deformation of the soft material by the rough surface asperities (Persson, 1998). These effects were minimized here as the fixing process prevented contact between the soft tissue and test substrates, but in the wild, such interactions would further increase the ability of remora to remain attached to a surface. However, despite neglecting these effects, the ability of the spinules to enhance friction on rough surfaces demonstrates one manner in which the remora's attachment system is able to respond to uncertain attachment site conditions. Thus, the adaptation of spinules is one reason among many as to why remora can maintain attachment to such a wide variety of hosts.

Competing interests
The authors declare no competing or financial interests.

Author contributions
M.B., B.E.F. and J.H.N. developed the concepts and approach; M.B. performed experiments, data analysis, and prepared the manuscript; B.E.F. and J.H.N. assisted in interpretation of the results and edited the manuscript prior to submission.

Funding
This research was supported by internal funding from the Georgia Tech Research Institute and the Georgia Research Alliance.

References

ASTM (2014). *Standard Test Method for Static and Kinetic Coefficients of Friction of Plastic Film and Sheeting*, Vol. D1894. West Conshohocken, PA: ASTM International.

Barnes, W. J. P. (2007). Functional morphology and design constraints of smooth adhesive pads. *MRS Bull.* **32**, 479-485.

Bhushan, B. (2002). *Introduction to Tribology*. New York: John Wiley & Sons.

Bhushan, B. and Ruan, J.-A. (1994). Atomic-scale friction measurements using friction force microscopy: part II—application to magnetic media. *J. Tribol.* **116**, 389-396.

Bowden, F. P. and Tabor, D. (1950). *The Friction and Lubrication of Solids Part I*. London: Oxford University Press.

Britz, R. and Johnson, G. D. (2012). Ontogeny and homology of the skeletal elements that form the sucking disc of remoras (Teleostei, Echeneoidei, Echeneidae). *J. Morphol.* **273**, 1353-1366.

Brunnschweiler, J. M. (2005). Water-escape velocities in jumping blacktip sharks. *J. R. Soc. Interface* **2**, 389-391.

Cressey, R. F. and Lachner, E. A. (1970). The parasitic copepod diet and life history of diskfishes (Echeneidae). *Copeia* **1970**, 310-318.

Culler, M. and Nadler, J. H. (2014). Composite structural mechanics of dorsal lamella in remora fish. 2013 MRS Fall Meeting. *MRS Online Proceedings Library*, **1619**.

Culler, M., Ledford, K. A. Nadler, J. H. (2014). The role of topology and tissue mechanics in remora attachment. 2013 MRS Fall Meeting. *MRS Online Proceedings Library*, **1648**.

Fulcher, B. A. and Motta, P. J. (2006). Suction disk performance of Echeneid fishes. *Can. J. Zool.* **84**, 42-50.

Gibson, R. N. (1969). Powers of adhesion in *Liparis montagui* (Donovan) and other shore fish. *J. Exp. Mar. Biol. Ecol.* **3**, 179-190.

Green, D. M. and Barber, D. L. (1988). The ventral adhesive disc of the clingfish *Gobiesox maeandricus*: integumental structure and adhesive mechanisms. *Can. J. Zool.* **66**, 1610-1619.

Hora, S. L. (1923). The adhesive apparatus of the “sucking-fish”. *Nature* **111**, 668-668.

Maie, T., Schoenfuss, H. L. and Blob, R. W. (2012). Performance and scaling of a novel locomotor structure: adhesive capacity of climbing Gobiid fishes. *J. Exp. Biol.* **215**, 3925-3936.

Makinson, K. R. (1948). On the cause of the frictional difference of the wool fibre. *Trans. Faraday Soc.* **44**, 279-282.

Motta, P., Habegger, M. L., Lang, A., Hueter, R. and Davis, J. (2012). Scale morphology and flexibility in the shortfin mako *Isurus oxyrinchus* and the blacktip shark *Carcharhinus limbatus*. *J. Morphol.* **273**, 1096-1110.

Muir, B. S. and Buckley, R. M. (1967). Gill ventilation in *Remora remora*. *Copeia* **1967**, 581-586.

Nadler, J. H., Mercer, A. J., Culler, M., Ledford, K. A., Bloomquist, R. and Lina, A. (2013). Structures and function of remora adhesion. 2012 MRS Fall Meeting. *MRS Online Proceedings Library*, **1498**.

Persson, B. N. J. (1998). On the theory of rubber friction. *Surf. Sci.* **401**, 445-454.

Persson, B. N. J., Albohr, O., Tartaglino, U., Volokitin, A. I. and Tosatti, E. (2005). On the nature of surface roughness with application to contact mechanics, sealing, rubber friction and adhesion. *J. Physics* **17**, R1-R62.

Ritter, E. K. (2002). Analysis of sharksucker, Echeneis naucrates, induced behavior patterns in the blacktip shark, *Carcharhinus limbatus*. *Environ. Biol. Fishes* **65**, 111-115.

Ritter, E. K. and Brunnschweiler, J. M. (2003). Do sharksuckers, *Echeneis naucrates*, induce jump behaviour in blacktip sharks, *Carcharhinus limbatus*? *Mar. Freshw. Behav. Physiol.* **36**, 111-113.

Sazima, I. and Grossman, A. (2006). Turtle riders: remoras on marine turtles in southwest atlantic. *Neotrop. Ichthyol.* **4**, 123-126.

Schwartz, F. J. (1977). Effects of the sharksucker, *Echeneis naucrates*, disk on scaled and scaleless fish and sea turtles. *ASB Bull.* **24**, 84.

Schwartz, F. J. (1992). Effects of the sharksucker, *Echeneis naucrates*, family Echeneididae, on captive sheepshead, Archosargus probatocephalus. *J. Elisha Mitchell Sci. Soc.* **108**, 55-56.

Sewell, R. B. S. (1925). The adhesive apparatus of the “sucking-fish”. *Nature* **115**, 48-49.

Silva, J. M., Jr and Sazima, I. (2003). Whalesuckers and a spinner dolphin bonded for weeks: does host fidelity pay off? *Biota Neotrop.* **3**, 1-5.

Stote, A., Kenaley, C. P. and Flammang, B. E. (2014). A morphological analysis of the suction-disc performance and interspecific host association in the remoras (Percomorpha: Carangiformes: Echeneidae). *Integr. Comp. Biol.* **54**, E355-E355.

Strasburg, D. W. (1962). Some aspects of the feeding behavior of *Remora remora*. *Pac. Sci.* **16**, 202-206.

Vorburger, T. V. (1992). *Methods for Characterizing Surface Topology*. Washington, DC: Optical Society of America.

Wainwright, D. K., Kleinteich, T., Kleinteich, A., Gorb, S. N. and Summers, A. P. (2013). Stick tight: suction adhesion on irregular surfaces in the northern clingfish. *Biol. Lett.* **9**, 20130234.

Webb, P. W. and Keyes, R. S. (1982). Swimming kinematics of sharks. *Fishery Bull.* **80**, 803-812.

Weihs, D., Fish, F. E. and Nicastro, A. J. (2007). Mechanics of remora removal by dolphin spinning. *Mar. Mamm. Sci.* **23**, 707-714.

Williams, E. H., Jr, Mignucci-Giannoni, A. A., Bunkley-Williamsss, L., Bonde, R. K., Self-Sullivan, C., Preen, A. and Cockcroft, V. G. (2003). Echeneid-Sirenian associations, with information on sharksucker diet. *J. Fish Biol.* **63**, 1176-1183.

Journal of Experimental Biology